Dual-Site Synergistic Passivation for $CsPbBr_3$ Perovskite Solar Cells with Record 1.707 V V_{oc} and 11.23% Efficiency

Yinping Teng,[a] Yuanyuan Zhao,*[b] Zhe Xin,[a] Liqiang Bian,[b] Qiyao Guo,[c] Jialong Duan,[c] Jie Dou,[c] Yan Zhang,[d] Qiang Zhang[a] and Qunwei Tang*[c]

[a] *College of Mechanical and Electronic Engineering, Shandong University of Science and Technology, Qingdao 266590, PR China.*

[b] *College of Energy Storage Technology, Shandong University of Science and Technology, Qingdao 266590, PR China*

[c] *Institute of Carbon Neutrality, College of Chemical and Biological Engineering, Shandong University of Science and Technology, Qingdao 266590, PR China.*

[d] *College of Chemistry, Chemical Engineering and Materials Science, Shandong Normal University, Jinan 250014, PR China.*

* Corresponding author.

E-mail address: yuanyuanzhao@sdust.edu.cn (Y. Z.), tangqunwei@sdust.edu.cn (Q. T.)

Experimental Section

***Materials*:** Stannous chloride anhydrous ($SnCl_2$, Aladdin), thiourea (CH_4N_2S, Aladdin), lead bromide ($PbBr_2$, Aladdin), cesium bromide (CsBr, Aladdin), N,N-dimethylformamide (DMF, Sinopharm), titanium tetrachloride ($TiCl_4$, Sinopharm), methanol (CH_3OH, Sinopharm), isopropanol (C_3H_8O, Sinopharm), bis(diphenylphosphino)methane ($C_{25}H_{22}P_2$, Aladdin), 1,3-bis(diphenylphosphino)propane ($C_{27}H_{26}P_2$, Aladdin), 1,5-bis(diphenylphosphino)pentane ($C_{29}H_{30}P_2$, Aladdin), [6,6]-phenyl-C61-butyric acid methyl ester ($PC_{61}BM$, Polymer), FTO glass (7 Ω square^{-1}) and carbon paste (Shanghai Mater Win New Materials Co., Ltd) were used as supplied without further purification.

***Device fabrication*:** The FTO/glass substrates were sequentially cleaned with cleaning agent, deionized water, and anhydrous ethanol under ultrasonication. The cleaned FTO substrate and SnO_2 QDs solution were preheated at 80 °C for 5 min. The preheated SnO_2 QDs solution was spin-coated on FTO substrate at 2000 rpm for 30 s, and annealed at 200 °C for 1 h to obtain a dense SnO_2 ETL. The TiO_xCl_{4-2x} modification was performed by soaking the SnO_2 coated FTO glass in 40 mM $TiCl_4$ aqueous solution at 75 °C for 30 min, and the substrates were rinsed with deionized water and ethanol, and then dried in air at 200 °C for 30 min. The fabrication of the $CsPbBr_3$ film was accomplished using a multistep spin-coating approach.[1] At last, a conductive carbon paste was coated onto $CsPbBr_3$ layer and annealed at 90 °C for 15 min.

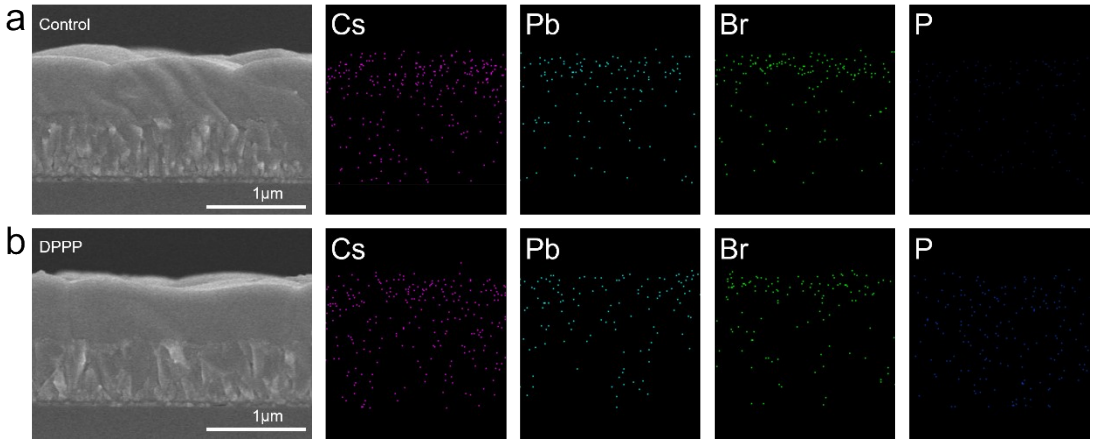

Fig. S1. The cross-sectional EDS mapping images of (a) control and (b) DPPP-treated perovskite film.

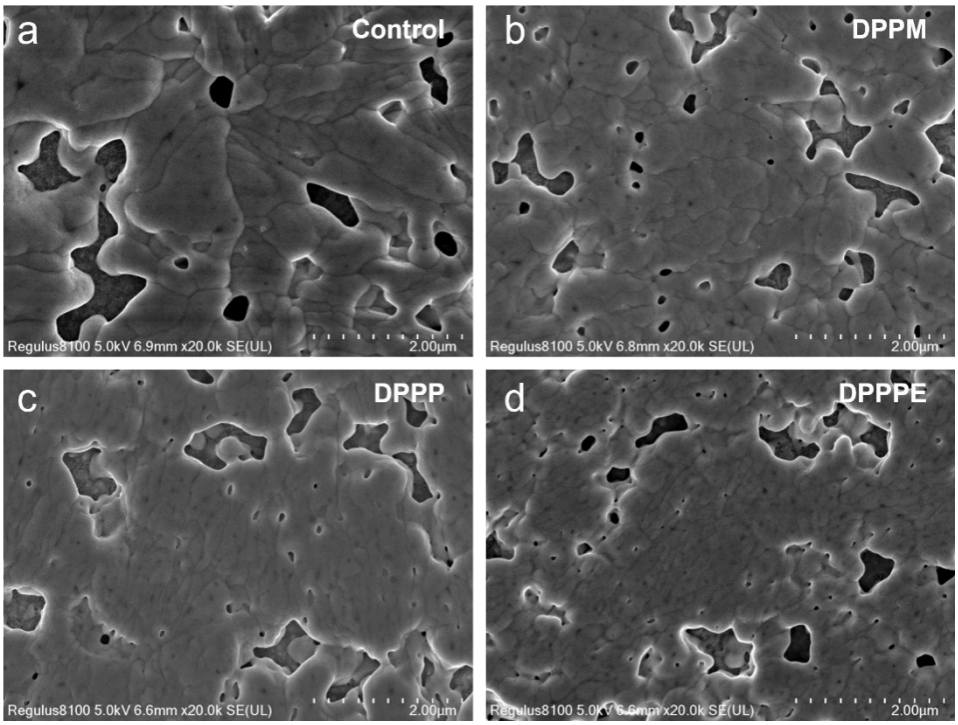

Fig. S2. The top-SEM of (a) control and $PbBr_2$ films treated with (b) DPPM, (c) DPPP, (d) DPPPE.

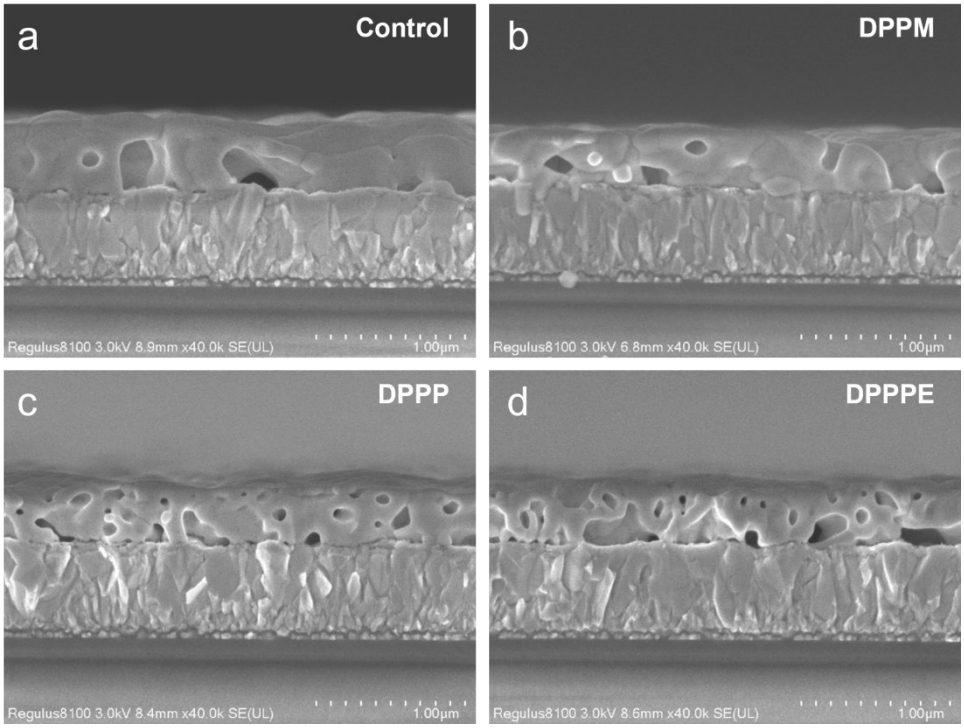

Fig. S3. The cross-SEM of (a) control and $PbBr_2$ films treated with (b) DPPM, (c) DPPP, (d) DPPPE.

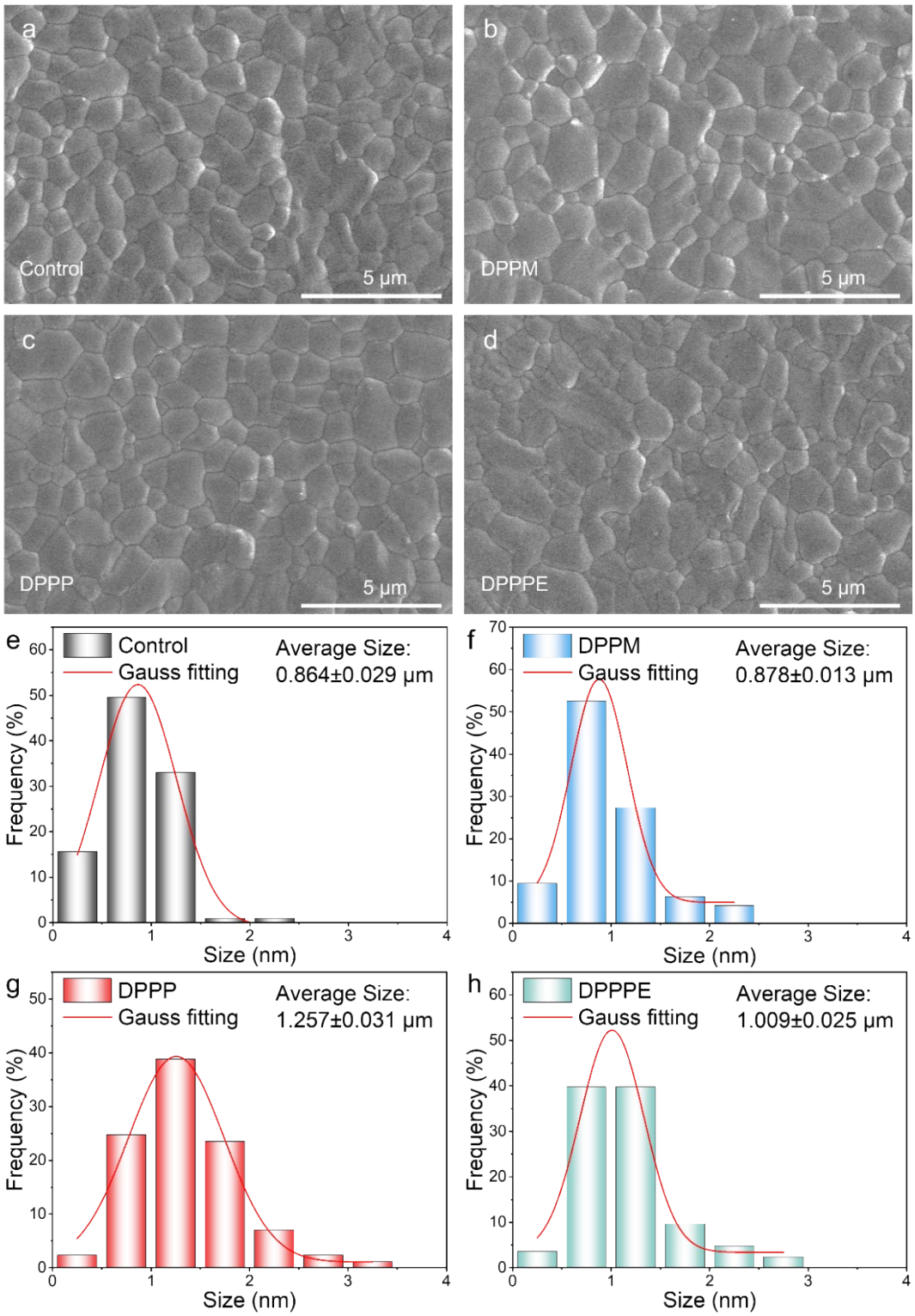

Fig. S4. Top-view SEM of (a) control and perovskite films treated with (b) DPPM, (c) DPPP, (d) DPPPE. (e-h) Corresponding grain size statistical distribution histogram.

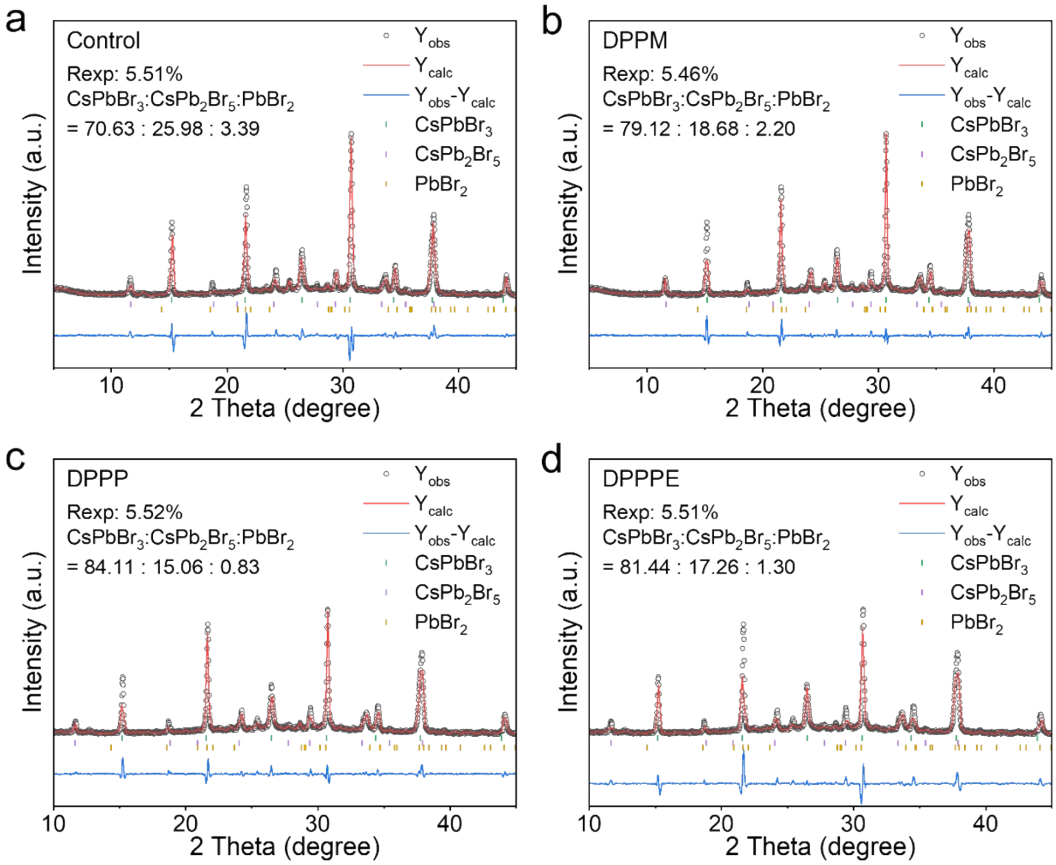

Fig. S5. XRD Rietveld refinement of (a) control and $CsPbBr_3$ films treated with (b) DPPM, (c) DPPP, (d) DPPPE.

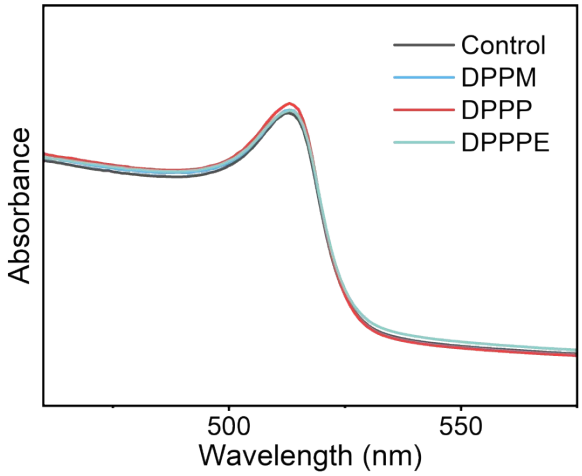

Fig. S6. The UV absorption spectra of different perovskite films.

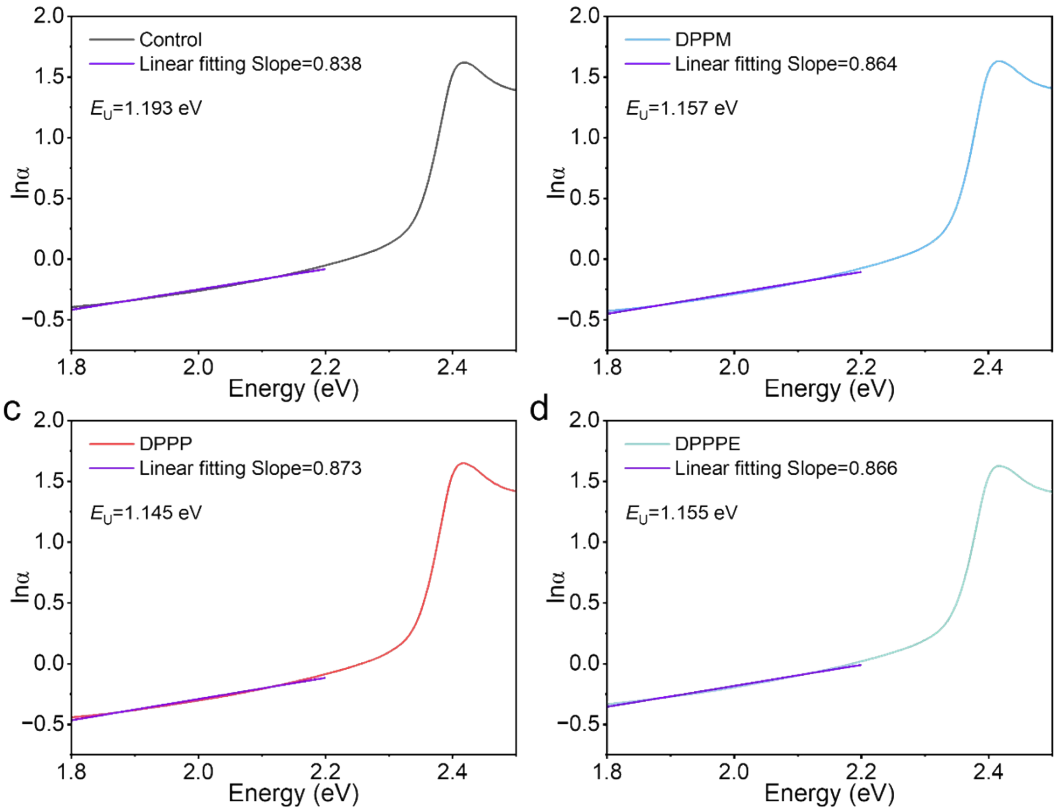

Fig. S7. Urbach energy calculation of (a) control and perovskite films treated with (b) DPPM, (c) DPPP, (d) DPPPE.

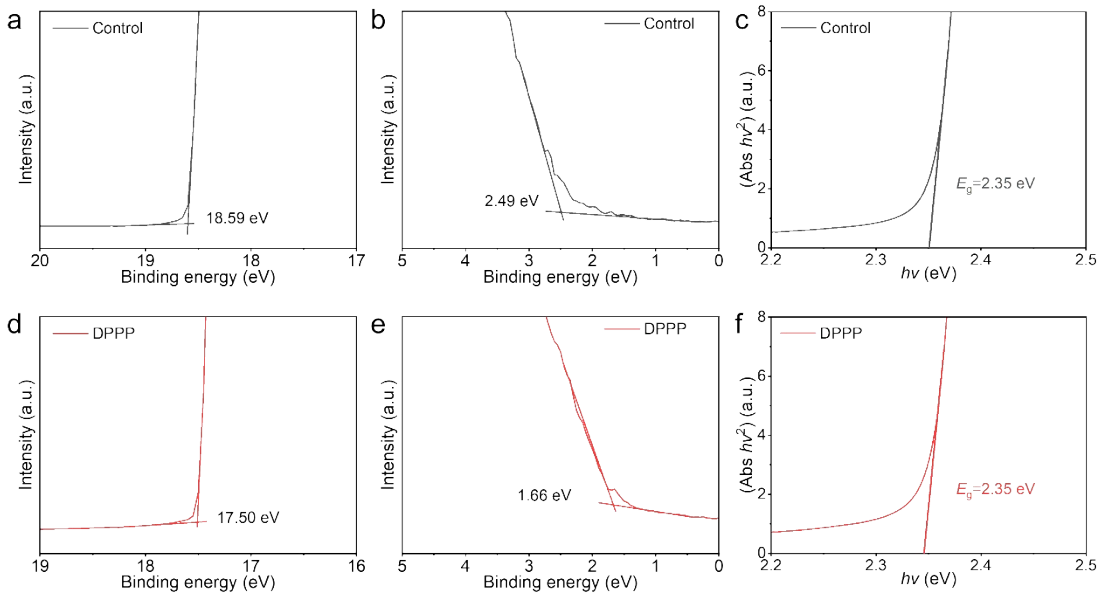

Fig. S8. (a) Secondary electron cut-off, (b) onset binding energies, (c) the calculation of the bandgap of control perovskite film. (d) Secondary electron cut-off, (e) onset binding energies, (f) the calculation of the bandgap of DPPP added perovskite film.

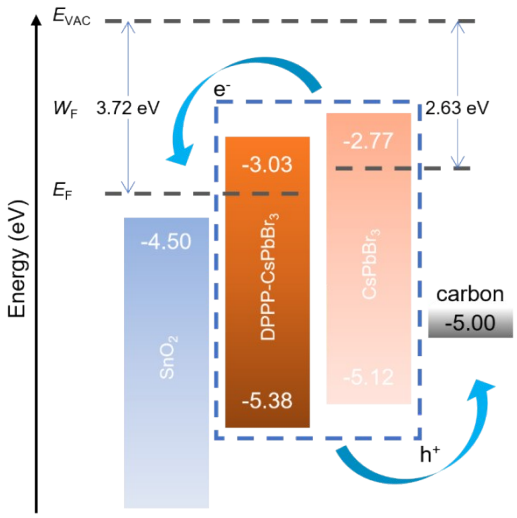

Fig. S9. Energy band diagram with and without DPPP treated.

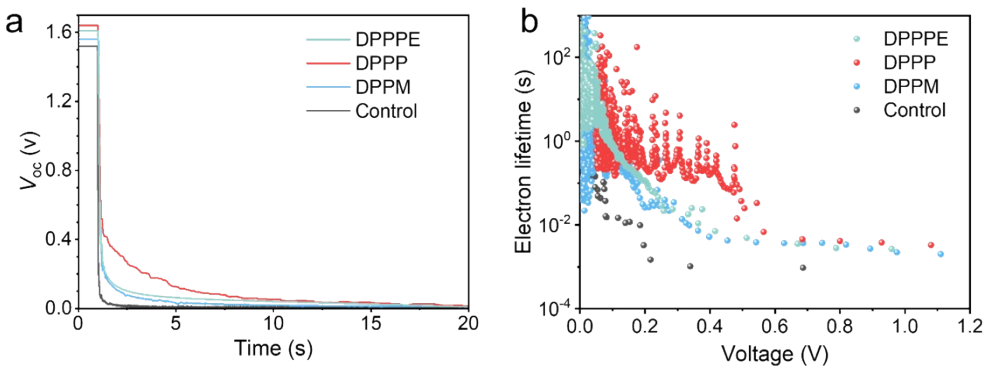

Fig. S10. (a) V_{oc} deacy curves and (b) electron lifetime (τ_n) plots of different PSCs.

The τ_n was calculated using the following equation:

$$\tau_n = -(kT/e) \times (dV_{oc}/dt)^{-1} \quad (1)$$

where k is the Boltzmann constant (1.38×10^{-23} J/K), e is the elementary charge (1.6×10^{-19} C) and T is the absolute temperature (298.15 K).

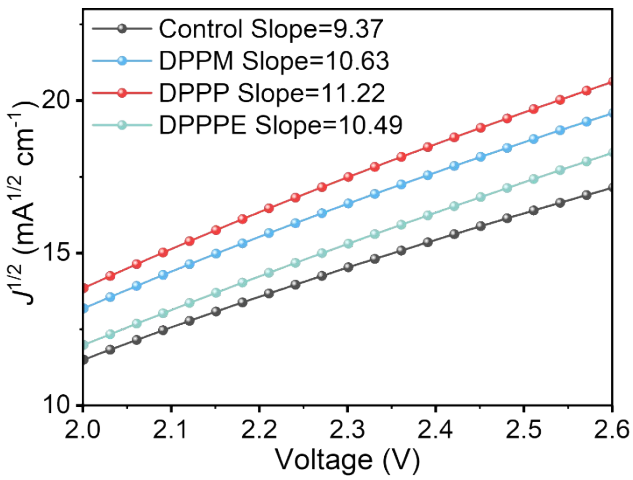

Fig. S11. The $J^{1/2}$ curves of different PSCs.

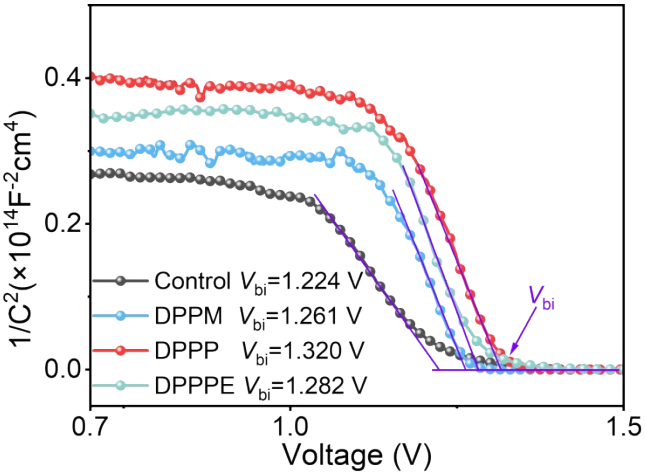

Fig. S12. Mott-Schottky (M-S) curves of different PSCs.

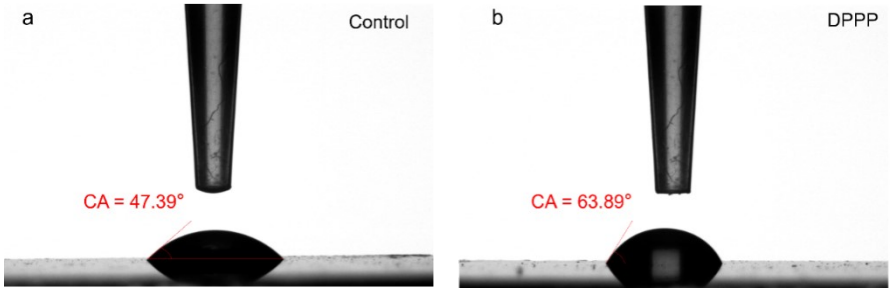

Fig. S13. Water contact angles of (a) control and perovskite films treated with (b) DPPP.

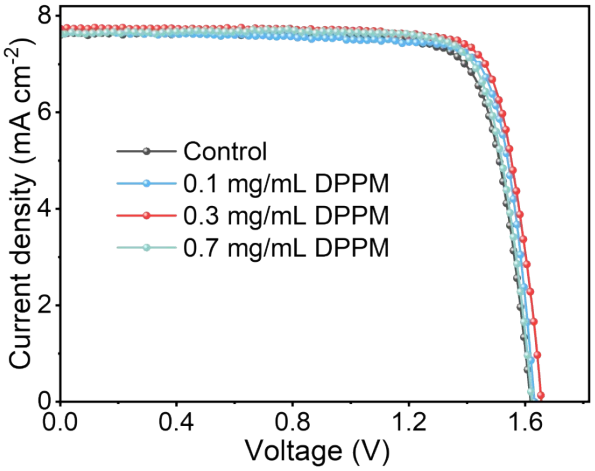

Fig. S14. *J-V* curves of the $CsPbBr_3$ PSCs fabricated with different concentrations of DPPM molecules.

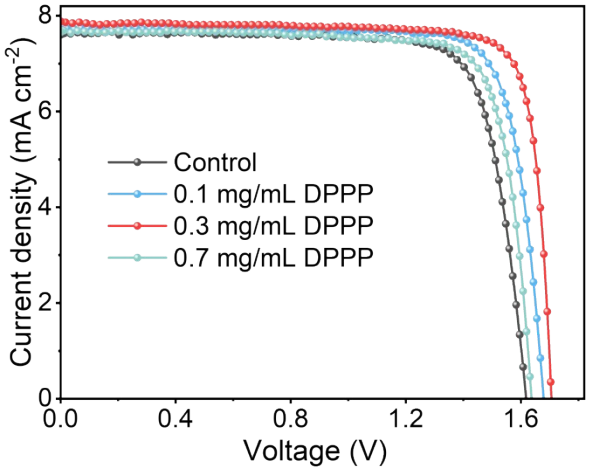

Fig. S15. *J-V* curves of the $CsPbBr_3$ PSCs fabricated with different concentrations of DPPP molecules.

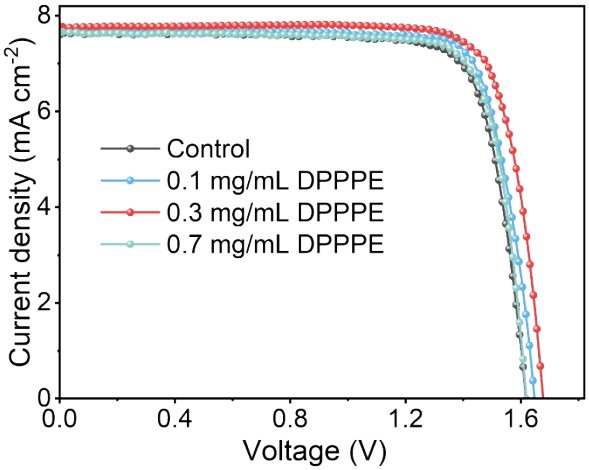

Fig. S16. *J-V* curves of the $CsPbBr_3$ PSCs fabricated with different concentrations of DPPPE molecules.

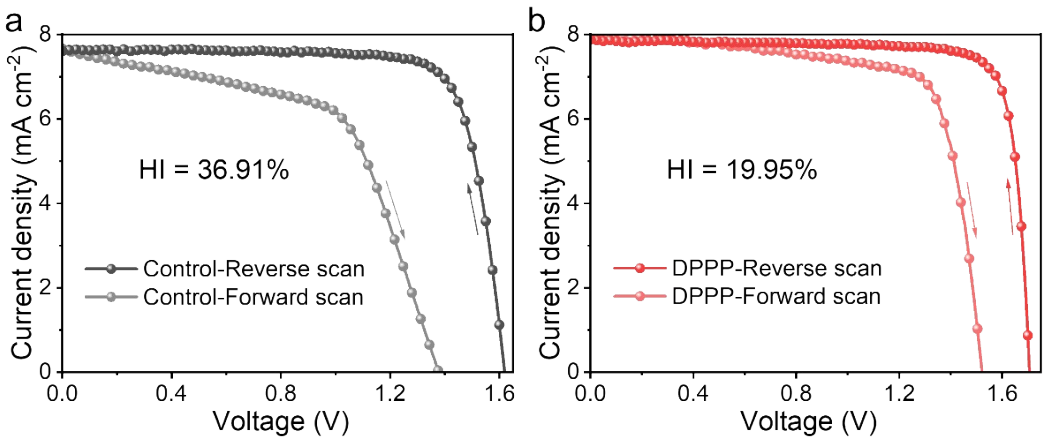

Fig. S17. Forward and reverse scan of (a) control and (b) DPPP-treated devices.

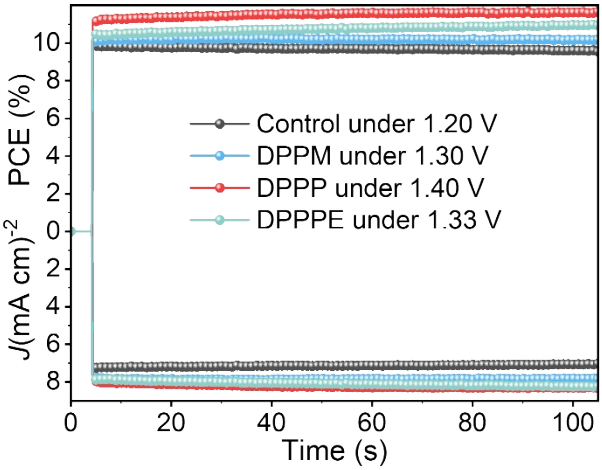

Fig. S18. Steady-state output curves of various $CsPbBr_3$ PSCs.

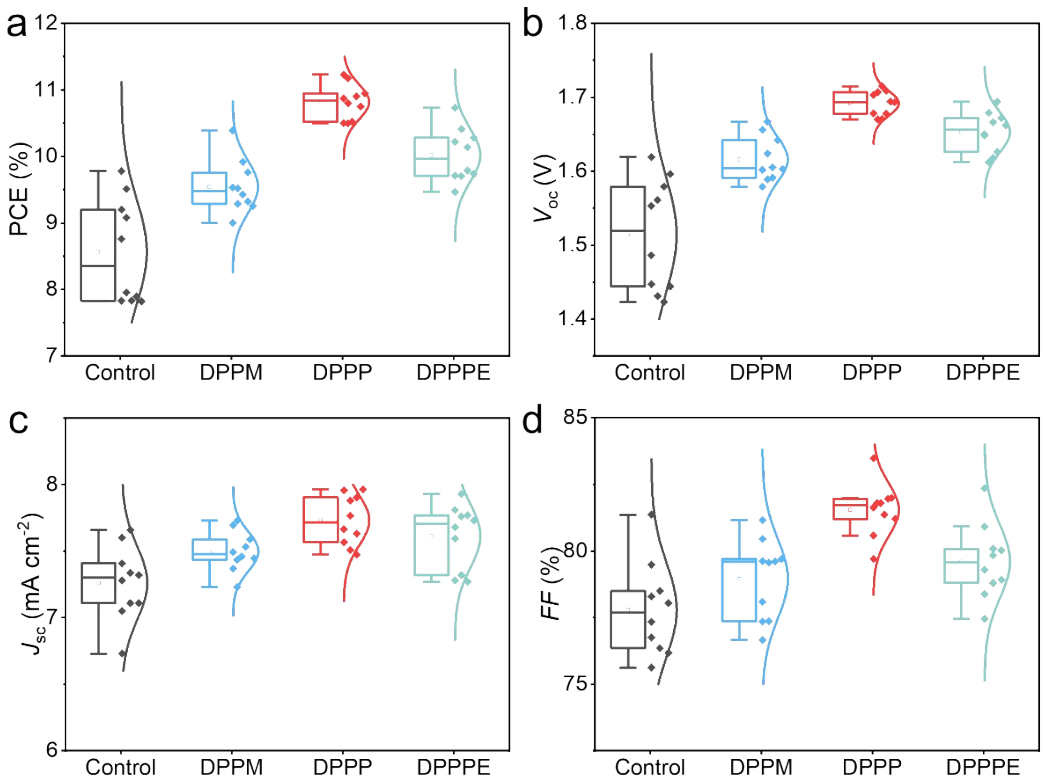

Fig. S19. Statistical (a) PCE, (b) V_{oc}, (c) J_{sc}, and (d) *FF* from ten random samples.

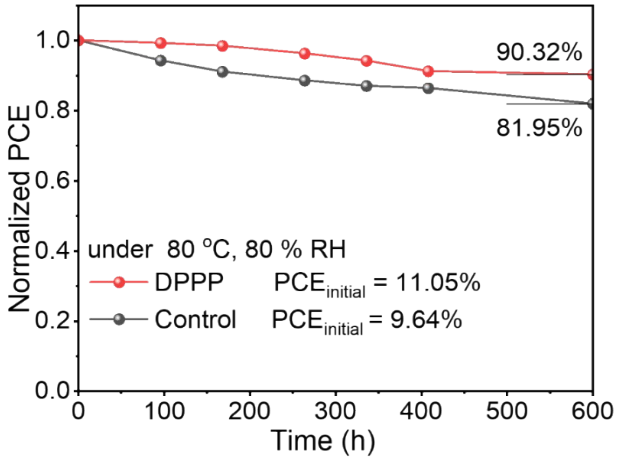

Fig. S20. Normalized PCE stability of the unencapsulated PSCs under 80 °C, 80% RH conditions.

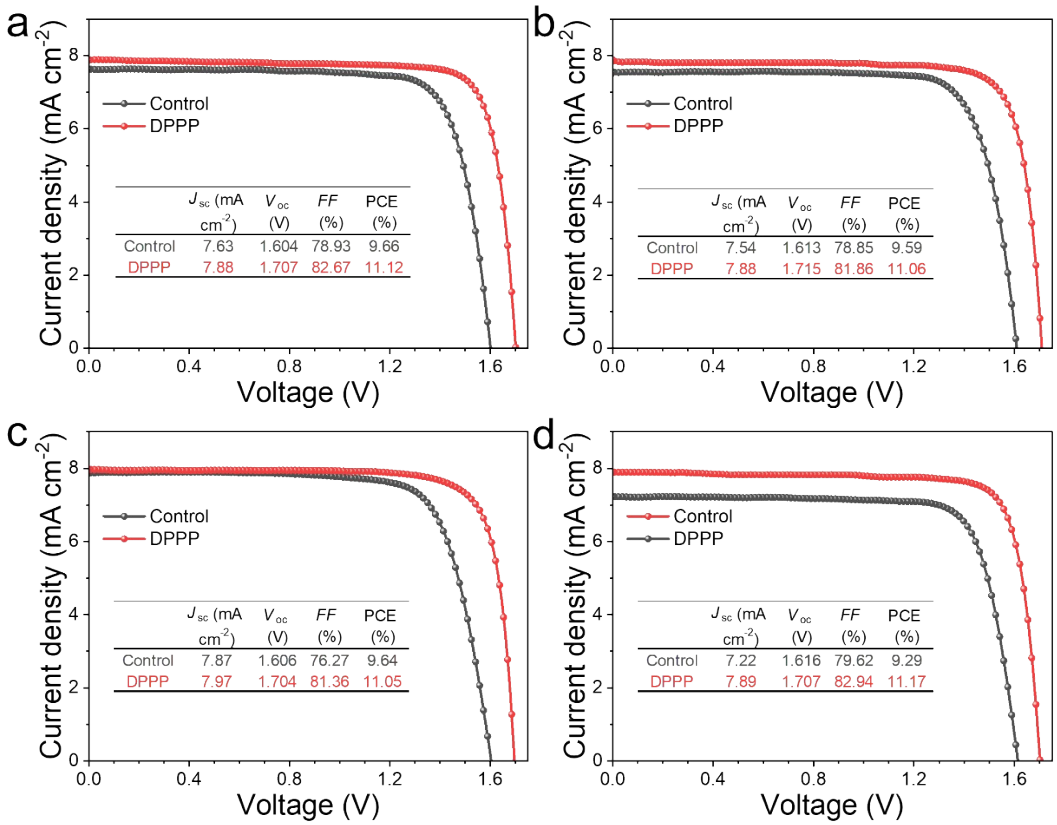

Fig. S21. The initial *J-V* curves of unencapsulated PSCs for stability tests under conditions of (a) high temperature, (b) high humidity, (c) high temperature and high humidity and (d) continuous LED illumination.

Table S1. The E_U value of perovskite films with and without the addition of DPPs.

Samples	E_U (eV)
Control	1.35
DPPM	1.28
DPPP	1.16
DPPPE	1.19

The E_U was calculation was computed using the data obtained from curve fitting, using the following equation:

$$\alpha = \alpha_0 exp\left(\frac{hv - E_g}{E_U}\right) \quad (2)$$

where α is the absorption coefficient as a function of photon energy hv (usually 21.22 eV), α_0 is the characteristic parameters of $CsPbBr_3$ (usually 5×10^4 cm^{-1}), E_g is is the optical band-gap of the $CsPbBr_3$ perovskite (2.35 eV).

Table S2. Energy band structure data of control and DPPP-treated perovskite films.

Samples	$E_{cut\text{-}off}$ (eV)	E_{onset} (eV)	E_{VB} (eV)	E_g (eV)	E_{CB} (eV)	W_F (eV)
Control	18.59	2.49	-5.12	2.35	-2.77	2.63
DPPP	17.50	1.66	-5.38	2.35	-3.03	3.72

The work function (W_F) can be calculated by equation: $W_F = hv - E_{cut\text{-}off}$, where hv is the excitation energy of UPS light source (usually 21.22 eV), $E_{cut\text{-}off}$ is the binding energy of the secondary electron cutoff edge.

The valence band top E_{VB} and the conduction band bottom E_{CB} are expressed as follow equations: $E_{VB} = -(W_F + E_{onset})$ and $E_{CB} = E_{VB} + E_g$, where E_{onset} is the starting edge energy, E_g is the optical band-gap of the perovskite.

Table S3. Carrier lifetime parameters of perovskite films with and without the addition of DPPs.

Samples	τ_{ave} (ns)	τ_1 (ns)	A_1 (%)	τ_2 (ns)	A_2 (%)
Control	0.62	0.08	28.01	0.82	71.99
DPPM	0.66	0.09	45.26	1.13	54.74
DPPP	1.87	5.32	25.37	0.61	74.63
DPPPE	0.83	0.13	25.06	1.06	74.94

The TRPL decay curves are fitted using a biexponential function as the following:

$$I = Ae^{-(\tau-\tau_0)/\tau_1} + Be^{-(\tau-\tau_0)/\tau_2} \quad (3)$$

where I is the PL intensity, $\tau_1$and τ_2 correspond to the fast decay time of the defect-induced non-radiative recombination and the low decay time of radiative recombination, respectively, and A and B are the corresponding decay constants.

The τ_{ave} can be calculated using the following equation:

$$\tau_{ave} = \left(A_1\tau_1^2 + A_2\tau_2^2\right)/\left(A_1\tau_1 + A_2\tau_2\right) \quad (4)$$

where τ_1 is the non-radiative fast decay lifetime, τ_2 is the radiative recombination slow decay lifetime, and A_1 and A_2 represent the amplitude.

Table S4. The V_{TFL}, N_t, and μ_e value of electron-only devices with and without the addition of DPPs.

Samples	V_{TFL} (V)	N_t (10^{15} cm^{-3})	μ_e (10^{-4} cm^2 V^{-1} s^{-1})
Control	1.382	9.330	8.7
DPPM	1.332	8.993	11.1
DPPP	1.264	8.534	12.4
DPPPE	1.294	8.736	10.9

The N_t was estimated from the trap-filled limited region using the following equation:

$$N_t = \frac{2V_{TFL}\varepsilon\varepsilon_0}{qL^2} \tag{5}$$

where V_{TFL}, ε, ε_0, and L represents the voltage onset in the trap-filled limited region, relative dielectric constant (22), vacuum permittivity (8.85×10^{-12} F m^{-1}), and L is the thickness of the film (550 nm), respectively.

The μ_e calculation was computed using the data obtained from curve fitting, using the following equation:

$$\mu_e = \frac{8J_D L^3}{9\varepsilon\varepsilon_0 V^2} \tag{6}$$

where J_D, V represents the dark current density, applied voltage, respectively.

Table S5. Photovoltaic performance of $CsPbBr_3$ PSCs with different concentrations of DPPM.

Samples	J_{sc} (mA cm^{-2})	V_{oc} (V)	*FF* (%)	PCE (%)
Control	7.60	1.619	79.48	9.78
0.1 mg/mL	7.68	1.632	80.74	10.12
0.3 mg/mL	7.73	1.656	81.17	10.39
0.7 mg/mL	7.65	1.623	80.06	9.94

Table S6. Photovoltaic performance of $CsPbBr_3$ PSCs with different concentrations of DPPP.

Samples	J_{sc} (mA cm^{-2})	V_{oc} (V)	*FF* (%)	PCE (%)
Control	7.60	1.619	79.48	9.78
0.1 mg/mL	7.72	1.679	81.55	10.57
0.3 mg/mL	7.88	1.707	83.48	11.23
0.7 mg/mL	7.65	1.638	80.77	10.12

Table S7. Photovoltaic performance of $CsPbBr_3$ PSCs with different concentrations of DPPPE.

Samples	J_{sc} (mA cm^{-2})	V_{oc} (V)	*FF* (%)	PCE (%)
Control	7.60	1.619	79.48	9.78
0.1 mg/mL	7.70	1.648	80.61	10.23
0.3 mg/mL	7.76	1.679	82.35	10.73
0.7 mg/mL	7.65	1.620	80.21	9.94

Table S8. Representative photovoltaic data for the inorganic $CsPbBr_3$ perovskite solar cells.

Year	Devices	J_{sc} (mA cm^{-2})	V_{oc} (V)	FF (%)	PCE (%)	Ref.
2024	FTO/SnO_2/$CsPbBr_3$-DPPP/carbon	7.88	1.707	83.48	11.23	This work
2024	FTO/PAA-SnO_2/PAA/$CsPbBr_3$/carbon	7.93	1.674	81.59	10.83	2
2024	FTO/TiO_2/G/$CsPbBr_3$/carbon	8.07	1.590	82.92	10.64	3
2024	FTO/SnO_2/TPA/$CsPbBr_3$/carbon	8.09	1.672	83.04	11.23	4
2024	FTO/SnO_2/TiO_xCl_{4-2x}/NH_4Cl-$CsPbBr_3$/carbon	7.96	1.650	80.80	10.61	5
2024	FTO/SnO_2/$CsPbBr_3$/CuS-MXene/carbon	7.76	1.629	83.14	10.51	6
2024	FTO/TiO_2/$CsPbBr_3$/MBA/CQDs/carbon	7.82	1.613	82.46	10.40	7
2023	FTO/TiO_2/ZnO/$CsPbBr_3$/carbon	9.01	1.580	75.00	10.67	8
2023	FTO/*c*-TiO_2/*m*-TiO_2/$CsPbBr_3$/(WS_2/$AgIn_5S_8$) QDs HTM/carbon	7.49	1.627	84.03	10.24	9
2023	FTO/TiO_2/DTPT/$CsPbBr_3$/DTPT/carbon	8.52	1.574	83.67	11.21	10
2023	FTO/SnO_2/$CsPbBr_3$/carbon	7.87	1.611	79.75	10.11	11
2022	FTO/*c*-TiO_2/*m*-TiO_2/Br-CQDs/$CsPbBr_3$-Br-CQDs/carbon	7.84	1.651	83.36	10.79	12
2022	FTO/SnO_2-SnS_2/$CsPbBr_3$/carbon	7.80	1.635	84.04	10.72	13
2022	FTO/*c*-TiO_2/*m*-TiO_2/EMImCl-$CsPbBr_3$/carbon	7.83	1.650	82.99	10.71	14
2022	FTO/TiO_2/$CsPbBr_3$/$ReSe_2$/carbon	7.92	1.622	83.06	10.67	15
2022	FTO/*c*-TiO_2/*m*-TiO_2/$CsPbBr_3$/DCC/carbon	7.79	1.611	80.96	10.16	16
2022	FTO/*c*-TiO_2/*m*-TiO_2/ASF/$CsPbBr_3$/carbon	7.47	1.615	83.56	10.08	17
2021	FTO/SnO_2-TiO_xCl_{4-2x}/$CsPbBr_3$+$Ti_3C_2Cl_x$/$Ti_3C_2Cl_x$/carbon	7.87	1.702	82.70	11.08	18
2021	FTO/L-TiO_2/$CsPbBr_3$/carbon	7.58	1.675	84.60	10.75	19

2021	FTO/2D SnO_2/GQDs/$CsPbBr_3$/carbon	7.94	1.585	82.20	10.34	20
2021	FTO/*c*-TiO_2/*m*-TiO_2/$CsPbBr_3$/Br-GO/carbon	7.88	1.602	80.01	10.10	21
2021	FTO/*c*-TiO_2/*m*-TiO_2/$CsPbBr_3$/carbon	7.69	1.568	79.70	9.61	22
2020	FTO/*c*-TiO_2/*m*-TiO_2/$CsPbBr_3$/$CuInS_2$/ZnS QDs/LPP-C	7.73	1.626	86.30	10.85	23
2020	FTO/SnO_2/$CsPbBr_3$/NCQDs/carbon	7.87	1.622	80.10	10.71	24
2020	FTO/SnO_2-TiO_xCl_{4-2x}/WS_2/$CsPbBr_3$/carbon	7.95	1.700	79.00	10.65	25
2020	FTO/SnO_2/TiO_xCl_{4-2x}/$Cs_{0.91}Rb_{0.09}PbBr_3$/carbon	7.96	1.629	80.50	10.44	26
2020	FTO/TiO_2/$CsPbBr_3$/[BMMIm]Cl/carbon	7.45	1.610	83.00	9.92	27
2019	FTO/SnO_2/$CsPbBr_3$/$CsSnBr_3$/carbon	7.80	1.610	84.40	10.60	1
2019	FTO/*c*-TiO_2/*m*-TiO_2/$CsPbBr_3$/Cu(Cr,Ba)O_2/carbon	7.81	1.615	85.50	10.79	28
2019	FTO/*c*-TiO_2/*m*-TiO_2/GQDs/$CsPbBr_3$/MnS/carbon	8.28	1.520	83.00	10.45	29
2019	FTO/*c*-TiO_2/*m*-TiO_2/$CsPbBr_3$/P1Z1/carbon	7.652	1.578	83.06	10.03	30
2019	FTO/*c*-TiO_2/*m*-TiO_2/$CsPb_{0.995}Zn_{0.005}Br_3$/carbon	7.30	1.560	80.61	9.18	31
2018	FTO/*c*-TiO_2/*m*-TiO_2/$CsPb_{0.97}Tb_{0.03}Br_3$/SnS:ZnS/NiO_x/carbon	8.21	1.570	79.60	10.26	32
2018	FTO/*c*-TiO_2/*m*-TiO_2/$CsPb_{0.97}Sm_{0.03}Br_3$/carbon	7.48	1.594	85.10	10.14	33
2018	FTO/*c*-TiO_2/*m*-TiO_2/GQDs/$CsPbBr_3$/carbon	8.12	1.458	82.10	9.72	34
2018	FTO/TiO_2/GQDs $CsPbBr_3$/CISZ-QDs/carbon	7.35	1.522	84.30	9.43	35
2018	FTO/*c*-TiO_2/*m*-TiO_2/GQDs/$CsPbBr_3$ CdZnSe@ZnSe/carbon	7.25	1.498	79.60	8.65	36
2017	FTO/TiO_2/CQD-$CsPbBr_3$ IO/Spiro-OMeTAD/Ag	11.34	1.060	69.00	8.29	37
2017	FTO/*c*-TiO_2/$CsPbBr_3$/Spiro-MeOTAD/Au	7.05	1.410	55.00	5.50	38
2016	FTO/*c*-TiO_2/*m*-TiO_2/$CsPbBr_3$/carbon	7.40	1.240	73.00	6.70	39
2016	FTO/*c*-TiO_2/*m*-TiO_2/$CsPbBr_3$/PTAA/Au	6.70	1.250	73.00	6.20	40

2016	FTO/*c*-TiO_2/$CsPbBr_3$/Spiro-MeOTAD/Au	5.65	1.536	62.40	5.42	41
2015	FTO/*m*-TiO_2/$CsPbBr_3$/Spiro-MeOTAD/Au	6.24	1.280	74.00	5.95	42

Table S9. Hysteresis *J-V* curves of control and DPPP-treated PSCs.

Samples	J_{sc} (mA cm^{-2})	V_{oc} (V)	*FF* (%)	PCE (%)	HI (%)
Control-Reverse scan	7.60	1.619	79.48	9.78	36.91
Control-Foeward scan	7.66	1.378	58.45	6.17	
DPPP-Reverse scan	7.88	1.707	83.48	11.23	19.95
DPPP-Forward scan	7.95	1.522	74.30	8.99	

Table S10. The fitting parameters of R_{rec} and R_{ct} of devices with and without the addition of DPPs were determined using the Z-View software. The R_{rec} and R_{ct} were obtained from the Nyquist plot under dark and light conditions, respectively.

Samples	R_{rec} (Ω)	R_{ct} (Ω)
Control	387.6	820.7
DPPM	2985	703.4
DPPP	9113	665.5
DPPPE	2687	719.7

References

1. Y. Zhao, J. Duan, H. Yuan, Y. Wang, X. Yang, B. He and Q. Tang, *Sol. RRL*, 2019, **3**, 1800284.
2. Y. Zhao, L. Gao, Q. Wang, Q. Zhang, X. Yang, J. Zhu, H. Huang, J. Duan and Q. Tang, *Carbon Energy*, 2024, **6**, e468.
3. Z. Wen, C. Liang, S. Li, G. Wang, B. He, H. Gu, J. Xie, H. Pan, Z. Su, X. Gao, G. Hong and S. Chen, *Energy Environ. Mater.*, 2024, **7**, e12680.
4. Q. Wang, J. Zhu, Y. Zhao, Y. Chang, N. Hao, Z. Xin, Q. Zhang, C. Chen, H. Huang and Q. Tang, *Carbon Energy*, 2024, **6**, e566.
5. Y. Zhao, Q. Wang, N. Hao, Q. Zhang, J. Zhu, H. Huang and Q. Tang, *ACS Mater. Lett.*, 2024, **6**, 345-352.
6. Z. Wang, B. He, M. Wei, W. Liu, X. Li, J. Zhu, H. Chen and Q. Tang, *Chem. Eng. J.*, 2024, **479**, 147736.
7. S. Zhang, J. He, X. Guo, J. Su, Z. Lin, J. Zhang, L. Guo, Y. Hao and J. Chang, *ACS Mater. Lett.*, 2023, **5**, 1497-1505.
8. W. Liu, X. Yao, B. He, H. Sui, M. Wei, H. Chen, J. Duan and Q. Tang, *J. Mater. Chem. A*, 2023, **11**, 20206-20214.
9. H. Sui, B. He, J. Ti, S. Sun, W. Jiao, H. Chen, Y. Duan, P. Yang and Q. Tang, *Chem. Eng. J.*, 2023, **455**, 140728.
10. R. Guo, J. Xia, H. Gu, X. Chu, Y. Zhao, X. Meng, Z. Wu, J. Li, Y. Duan, Z. Li, Z. Wen, S. Chen, Y. Cai, C. Liang, Y. Shen, G. Xing, W. Zhang and G. Shao, *J. Mater. Chem. A*, 2023, **11**, 408-418.
11. L. Gao, Y. Zhao, Y. Chang, K. Gao, Q. Wang, Q. Zhang and Q. Tang, *Chem. Eng. J.*, 2023, **469**, 143881.
12. J. Zhu, B. He, M. Wang, X. Yao, H. Huang, C. Chen, H. Chen, Y. Duan and Q. Tang, *Nano Energy*, 2022, **104**, 107920.
13. X. Yao, B. He, J. Zhu, J. Ti, L. Cui, R. Tui, M. Wei, H. Chen, J. Duan, Y. Duan and Q. Tang, *Nano Energy*, 2022, **96**, 107138.
14. J. Zhu, B. He, W. Zhang, R. Tui, H. Chen, Y. Duan, H. Huang, J. Duan and Q. Tang, *Adv. Funct. Mater.*, 2022, **32**, 2206838.
15. J. Zhu, B. He, X. Yao, H. Chen, Y. Duan, J. Duan and Q. Tang, *Small*, 2022, **18**, 2106323.
16. J. Zhu, Y. Liu, B. He, W. Zhang, L. Cui, S. Wang, H. Chen, Y. Duan and Q. Tang, *Chem. Eng. J.*, 2022, **428**, 131950.
17. L. Cui, B. He, Y. Ding, J. Zhu, X. Yao, J. Ti, H. Chen, Y. Duan and Q. Tang, *Chem. Eng. J.*, 2022, **431**, 134193.
18. Q. Zhou, J. Duan, J. Du, Q. Guo, Q. Zhang, X. Yang, Y. Duan and Q. Tang, *Adv. Sci.*, 2021, **8**, 2101418.
19. J. Duan, M. Wang, Y. Wang, J. Zhang, Q. Guo, Q. Zhang, Y. Duan and Q. Tang, *ACS Energy Lett.*, 2021, **6**, 2336-2342.
20. Y. Zhao, J. Zhu, B. He and Q. Tang, *ACS Appl. Mater. Interfaces*, 2021, **13**, 11058-11066.
21. X. Sun, B. He, J. Zhu, R. Zhu, H. Chen, Y. Duan and Q. Tang, *Chem. Eng. J.*, 2021, **412**, 128727.
22. J. Zhu, M. Tang, B. He, K. Shen, W. Zhang, X. Sun, M. Sun, H. Chen, Y. Duan and Q. Tang, *Chem. Eng. J.*, 2021, **404**, 126548.
23. J. Duan, Y. Wang, X. Yang and Q. Tang, *Angew. Chem. Int. Ed.*, 2020, **59**, 4391-4395.

24. Y. Zhao, J. Duan, Y. Wang, X. Yang and Q. Tang, *Nano Energy*, 2020, **67**, 104286.
25. Q. Zhou, J. Duan, X. Yang, Y. Duan and Q. Tang, *Angew. Chem. Int. Ed.*, 2020, **59**, 21997-22001.
26. Q. Zhou, J. Duan, Y. Wang, X. Yang and Q. Tang, *J. Energy Chem.*, 2020, **50**, 1-8.
27. W. Zhang, X. Liu, B. He, Z. Gong, J. Zhu, Y. Ding, H. Chen and Q. Tang, *ACS Appl. Mater. Interfaces*, 2020, **12**, 4540-4548.
28. J. Duan, Y. Zhao, Y. Wang, X. Yang and Q. Tang, *Angew. Chem. Int. Ed.*, 2019, **58**, 16147-16151.
29. X. Li, Y. Tan, H. Lai, S. Li, Y. Chen, S. Li, P. Xu and J. Yang, *ACS Appl. Mater. Interfaces*, 2019, **11**, 29746-29752.
30. Y. Liu, B. He, J. Duan, Y. Zhao, Y. Ding, M. Tang, H. Chen and Q. Tang, *J. Mater. Chem. A*, 2019, **7**, 12635-12644.
31. M. Tang, B. He, D. Dou, Y. Liu, J. Duan, Y. Zhao, H. Chen and Q. Tang, *Chem. Eng. J.*, 2019, **375**, 121930.
32. H. Yuan, Y. Zhao, J. Duan, Y. Wang, X. Yang and Q. Tang, *J. Mater. Chem. A*, 2018, **6**, 24324-24329.
33. J. Duan, Y. Zhao, X. Yang, Y. Wang, B. He and Q. Tang, *Adv. Energy Mater.*, 2018, **8**, 1802346.
34. J. Duan, Y. Zhao, B. He and Q. Tang, *Angew. Chem. Int. Ed.*, 2018, **57**, 3787-3791.
35. J. Duan, T. Hu, Y. Zhao, B. He and Q. Tang, *Angew. Chem. Int. Ed.*, 2018, **57**, 5746-5749.
36. Q. Li, J. Bai, T. Zhang, C. Nie, J. Duan and Q. Tang, *Chem. Commun.*, 2018, **54**, 9575-9578.
37. S. Zhou, R. Tang and L. Yin, *Adv. Mater.*, 2017, **29**, 1703682.
38. J. B. Hoffman, G. Zaiats, I. Wappes and P. V. Kamat, *Chem. Mater.*, 2017, **29**, 9767-9774.
39. J. Liang, C. Wang, Y. Wang, Z. Xu, Z. Lu, Y. Ma, H. Zhu, Y. Hu, C. Xiao, X. Yi, G. Zhu, H. Lv, L. Ma, T. Chen, Z. Tie, Z. Jin and J. Liu, *J. Am. Chem. Soc.*, 2016, **138**, 15829-15832.
40. M. Kulbak, S. Gupta, N. Kedem, I. Levine, T. Bendikov, G. Hodes and D. Cahen, *J. Phys. Chem. Lett.*, 2016, **7**, 167-172.
41. Q. A. Akkerman, M. Gandini, F. Di Stasio, P. Rastogi, F. Palazon, G. Bertoni, J. M. Ball, M. Prato, A. Petrozza and L. Manna, *Nat. Energy*, 2016, **2**, 16194.
42. M. Kulbak, D. Cahen and G. Hodes, *J. Phys. Chem. Lett.*, 2015, **6**, 2452-2456.